

# Attempt to distinguish long-range temporal correlations from the statistics of the increments by natural time analysis

P. A. Varotsos,<sup>1,2,\*</sup> N. V. Sarlis,<sup>1</sup> E. S. Skordas,<sup>2</sup> H. K. Tanaka,<sup>3</sup> and M. S. Lazaridou<sup>1</sup>

<sup>1</sup>*Solid State Section, Physics Department, University of Athens, Panepistimiopolis, Zografos 157 84, Athens, Greece*

<sup>2</sup>*Solid Earth Physics Institute, Physics Department, University of Athens, Panepistimiopolis, Zografos 157 84, Athens, Greece*

<sup>3</sup>*Earthquake Prediction Research Center, Tokai University 3-20-1, Shimizu-Orido, Shizuoka 424-8610, Japan*

(Received 25 February 2006; revised manuscript received 30 June 2006; published 23 August 2006)

Self-similarity may originate from two origins: i.e., the process memory and the process' increments "infinite" variance. A distinction is attempted by employing the natural time  $\chi$ . Concerning the first origin, we analyze recent data on seismic electric signals, which support the view that they exhibit infinitely ranged *temporal* correlations. Concerning the second, slowly driven systems that emit bursts of various energies  $E$  obeying the power-law distribution—i.e.,  $P(E) \sim E^{-\gamma}$ —are studied. An interrelation between the exponent  $\gamma$  and the variance  $\kappa_1 (\equiv \langle \chi^2 \rangle - \langle \chi \rangle^2)$  is obtained for the shuffled (randomized) data. For real earthquake data, the most probable value of  $\kappa_1$  of the shuffled data is found to be approximately equal to that of the original data, the difference most likely arising from temporal correlation. Finally, it is found that the differential entropy associated with the probability  $P(\kappa_1)$  maximizes for  $\gamma$  around  $\gamma \approx 1.6$ – $1.7$ , which is comparable to the value determined experimentally in diverse phenomena: e.g., solar flares, icequakes, dislocation glide in stressed single crystals of ice, etc. It also agrees with the  $b$  value in the Gutenberg-Richter law of earthquakes. In addition, the case of multiplicative cascades is studied in the natural time domain.

DOI: [10.1103/PhysRevE.74.021123](https://doi.org/10.1103/PhysRevE.74.021123)

PACS number(s): 05.40.-a, 91.30.Dk, 05.45.Tp, 89.75.-k

## I. INTRODUCTION

A large variety of natural systems exhibit irregular and complex behavior which at first looks erratic, but in fact possesses scale-invariant structure (e.g., [1,2]). A process  $\{X(t)\}_{t \geq 0}$  is called self-similar [3] if, for some  $H > 0$ ,

$$X(\alpha t) = \alpha^H X(t) \quad \forall \alpha > 0, \quad (1)$$

where the symbol of equality refers here to all finite-dimensional distributions of the process on the left and right, and the parameter  $H$  is called the self-similarity index or exponent. Equation (1) means a "scale invariance" of the finite-dimensional distributions of  $X(t)$ , which does *not* imply, in stochastic processes, the same for the sample paths (e.g., [4]). Examples of self-similar processes are Brownian, fractional Brownian (fBm), and Lévy stable and fractional Lévy stable motion (fLsm). Lévy stable distributions (which are followed by many natural processes—e.g., [5,6]) differ greatly from the Gaussian ones because they have heavy tails and their variance is infinite (e.g., [4,7]).

An important point in analyzing data from natural systems that exhibit scale-invariant structure is the following: In several systems this nontrivial structure points to long-range *temporal* correlations; in other words, the self-similarity results from the process' memory *only* (e.g., the case of fBm). Alternatively, the self-similarity may solely result from the process' increments infinite variance: e.g., Lévy stable motion. (Note that in distributions that are applicable to a large variety of problems, extreme events have to be *truncated* for physical reasons—e.g., finite size effects—when there is no infinity [8], and this is why we write hereafter "infinite.") In general, however, the self-similarity may result from both

these origins (e.g., fLsm). It is the main aim of this paper to discuss how a distinction of the two origins of self-similarity (i.e., process' memory, process' increments "infinite" variance) can be in principle achieved by employing the natural time analysis.

Before proceeding, the following clarifications are necessary as far as the aforementioned two sources of self-similarity are concerned. Long-range temporal correlations, which are quoted above as a first origin of self-similarity, are an immediate consequence of Eq. (1) with  $H > \frac{1}{2}$  defining a self-similar process. We stress, however, that long-range correlations do not automatically imply self-similarity of a process. Multifractal processes provide a large class of counterexamples. Here, for example, we discuss the natural time analysis of multiplicative cascades in Sec. IV. The second origin of self-similarity comes from the statistical properties of the increments of the process. We emphasize, however, that the statistics of these increments does not automatically lead to nontrivial self-similarity of the process. Specifically, a process which is invariant under shuffling of the increments has independent increments and is characterized by the self-similarity index  $\frac{1}{2}$ .

In a time series comprising  $N$  events, the *natural time*  $\chi_k = k/N$  serves as an index [9,10] for the occurrence of the  $k$ th event. The evolution of the pair  $(\chi_k, Q_k)$  is considered [9–19], where  $Q_k$  denotes in general a quantity proportional to the energy released in the  $k$ th event. For example, for dichotomous signals  $Q_k$  stands for the duration of the  $k$ th pulse while for the seismicity  $Q_k$  is proportional to the seismic energy released during the  $k$ th earthquake [9,17,19] (which is proportional to the seismic moment  $M_0$ ). The normalized power spectrum  $\Pi(\omega) \equiv |\Phi(\omega)|^2$  was introduced [9,10], where

\*Electronic address: pvaro@otenet.gr

$$\Phi(\omega) = \sum_{k=1}^N p_k \exp\left(i\omega \frac{k}{N}\right) \quad (2)$$

and  $p_k = Q_k / \sum_{n=1}^N Q_n$ ,  $\omega = 2\pi\phi$ ;  $\phi$  stands for the *natural frequency*. When the system enters the *critical stage*, the following relation holds [9,10]:

$$\Pi(\omega) = \frac{18}{5\omega^2} - \frac{6\cos\omega}{5\omega^2} - \frac{12\sin\omega}{5\omega^3}. \quad (3)$$

For  $\omega \rightarrow 0$ , Eq. (3) leads to [9,10,16]  $\Pi(\omega) \approx 1 - 0.07\omega^2$  which reflects [17] the fact that the variance of  $\chi$  is given by  $\kappa_1 = \langle \chi^2 \rangle - \langle \chi \rangle^2 = 0.07$ , where  $\langle f(\chi) \rangle = \sum_{k=1}^N p_k f(\chi_k)$ . It has been argued [17] that in the case of earthquakes,  $\Pi(\phi)$  for  $\phi \rightarrow 0$  can be considered as an order parameter and the corresponding probability density distribution function (PDF) is designated by  $P[\Pi(\phi)]$ . Since, at  $\phi \rightarrow 0$ ,  $\kappa_1$  is linearly related to  $\Pi(\phi)$  [because Eq. (2) leads to  $\Pi(\phi) = 1 - 4\pi^2\phi^2\kappa_1$  for  $\phi \rightarrow 0$ ], one can study, instead of  $P[\Pi(\phi)]$ , the PDF of  $\kappa_1$ : i.e.,  $P(\kappa_1)$ . This will be used here. The entropy  $S$  in the natural time domain is defined as [9,12]  $S \equiv \langle \chi \ln \chi \rangle - \langle \chi \rangle \ln \langle \chi \rangle$ , which depends on the sequential order of events [13,14], and for infinitely ranged temporal correlations its value is smaller [12,16] than the value  $S_u = (\ln 2)/2 - 1/4 \approx 0.0966$  of a “uniform” distribution (defined in Refs. [9,11–14]—e.g., when all  $p_k$  are equal): i.e.,  $S < S_u$ . The value of the entropy obtained [15] upon considering the time reversal  $\mathcal{T}$ —i.e.,  $\mathcal{T}p_k = p_{N-k+1}$ —is labeled by  $S_-$ .

The paper is organized as follows: In Sec. II, we treat the case when solely long-range temporal correlations exist. Section III deals with the self-similarity resulting from the process’ increments infinite variance by restricting ourselves to slowly driven systems that emit energy bursts obeying power-law distributions. The analysis in the natural time domain of multiplicative cascades is treated in Sec. IV. A brief discussion follows in Sec. V, while Sec. VI presents the main conclusion. Three appendixes clarify some points discussed in the main text.

## II. CASE OF TEMPORAL CORRELATIONS

We consider here the case of seismic electric signal (SES) activities (*critical dynamics*) which exhibit infinitely ranged temporal correlations [10–12] and present below two recent examples.

As a first example, Fig. 1(a) shows a recent SES activity recorded at a station located in central Greece (close to Patras city, PAT) on 13 February 2006. It comprises 37 pulses, the durations  $Q_k$  of which vary between 1 s and 40 s [see Fig. 1(b)]. The natural time representation of this SES activity can be seen in Fig. 1(b), and the computation of  $\kappa_1$ ,  $S$ , and  $S_-$  leads to the following values:  $\kappa_1 = 0.072 \pm 0.002$ ,  $S = 0.080 \pm 0.002$ , and  $S_- = 0.078 \pm 0.002$ . These values obey the conditions  $\kappa_1 \approx 0.070$  and  $S, S_- < S_u$ , which have already been found [10,12,18] to be obeyed for other SES activities [this classification of the signal in Fig. 1(a) as SES activity was strikingly confirmed after the submission of the present paper; see Appendix A and Ref. [20]]. If we repeat the computation for surrogate data obtained by *shuffling* the dura-

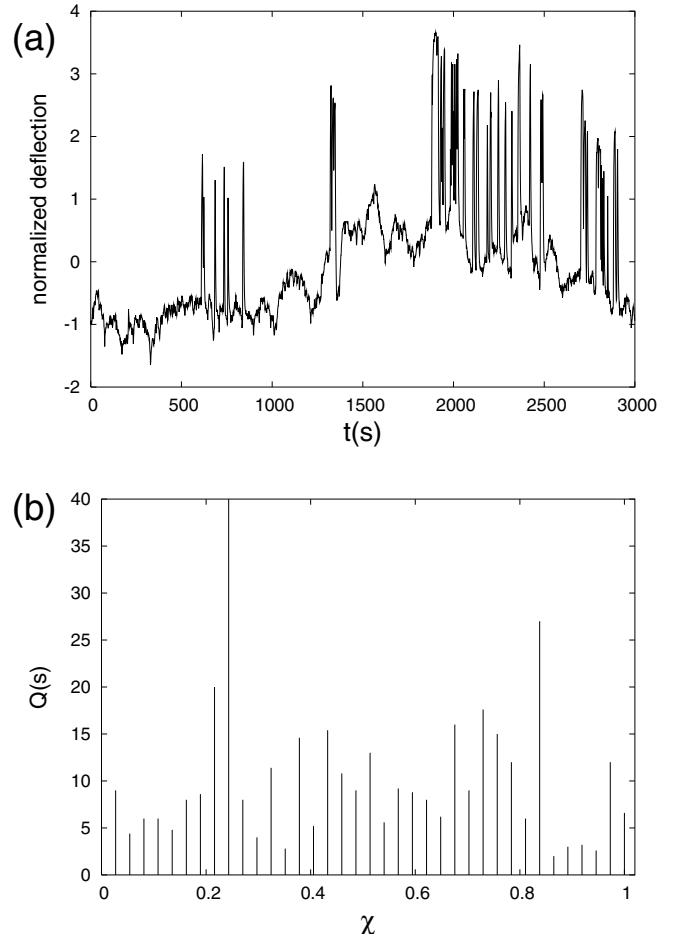


FIG. 1. (a) An SES activity recently recorded at PAT station (sampling rate  $f_{\text{expt}} = 1$  Hz). The actual electric field  $\mathbf{E}$  is [20] 6 mV/km, but here the signal is presented in normalized units—i.e., by subtracting the mean value and dividing by the standard deviation. (b) How the SES activity in (a) is read in natural time.

tions  $Q_k$  randomly (and hence their distribution is conserved), the corresponding quantities, designated by adding a subscript “shuf,” have the following values:  $\kappa_{1,\text{shuf}} = 0.082$  and  $S_{\text{shuf}} (=S_{-\text{shuf}}) = 0.091$  with standard deviations 0.008 and 0.011, respectively. They are almost equal to the corresponding values of a “uniform” distribution: i.e.,  $\kappa_u = 1/12 \approx 0.0833$  and  $S_u = 0.0966$ .

As a second example, Fig. 2(a) shows a more recent SES activity recorded again at PAT on 13 April 2006 (this will be hereafter called PAT<sub>2</sub>; see also Ref. [20]). It comprises 11 pulses only, the durations  $Q_k$  of which lead to the natural time representation depicted in Fig. 2(b) (other examples of SES activities that were recorded on 19 and 21 April 2006 are given in Ref. [20]). For the sake of the reader’s convenience, the dichotomous representation of the signal is also marked in Fig. 2(a). The computation of  $\kappa_1$ ,  $S$ , and  $S_-$  leads to the following values:  $\kappa_1 = 0.075 \pm 0.002$ ,  $S = 0.074 \pm 0.002$ , and  $S_- = 0.078 \pm 0.002$  which more or less obey the aforementioned conditions already found for other SES activities. After shuffling the durations  $Q_k$  randomly, we find  $\kappa_{1,\text{shuf}} = 0.082$  and  $S_{\text{shuf}} (=S_{-\text{shuf}}) = 0.084$  with standard deviations 0.007 and 0.008, respectively. Note that, as shown in Fig. 1

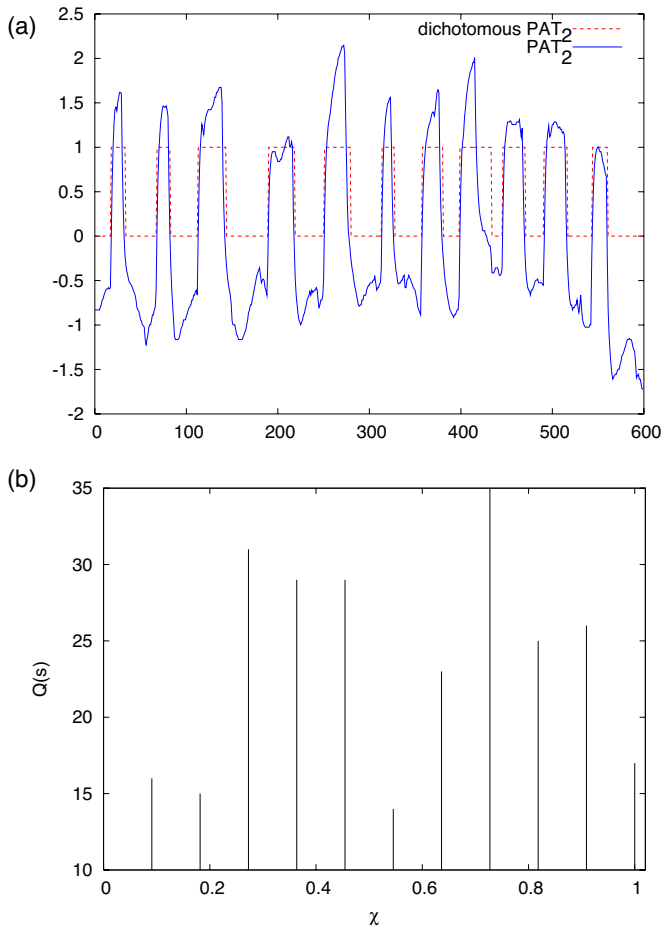


FIG. 2. (Color online) (a) An SES activity (solid blue line), PAT<sub>2</sub>, comprising 11 pulses only, which has been recorded at PAT on 13 April 2006. It is presented here in normalized units as the case of Fig. 1(a) (for other more recent examples see Ref. [20]) along with the corresponding dichotomous representation (dotted red line). (b) How the SES activity in (a) is read in natural time. Note that in the eighth pulse of (a), it seems that the dichotomous representation might overestimate  $Q_8$ . If we decrease this value by a factor of 2, the resulting  $\kappa_1$ ,  $S$ , and  $S_-$  become 0.076, 0.075, and 0.078, respectively, which agree within the experimental error with the corresponding values reported in Table I.

of Ref. [21], the  $S_u$  value of a “uniform” distribution comprising a very small number of pulses, as in the present case, is markedly smaller than 0.0966, being comparable to the value 0.084 found here if the experimental error is also taken into account.

By applying the same procedure to other SES activities reported earlier [15], we find (see Table I) that actually  $\kappa_{1,shuf} \approx \kappa_u$  and  $S_{shuf} \approx S_{-,shuf} \approx S_u$ . This points to the conclusion that the self-similarity of SES activities result from the process’ memory only (see also Appendix B), which agrees with the independent analysis of Ref. [4].

In addition, the detrended fluctuation analysis (DFA) [22,23] in natural time of the SES activity depicted in Fig. 1 leads to an exponent  $\alpha_{DFA} = 1.07 \pm 0.36$ , which agrees with the earlier finding  $\alpha_{DFA} \approx 1$  in several other SES activities [11] [the SES activity of Fig. 2(a) cannot lead to a reliable  $\alpha_{DFA}$  due to the very small number of pulses]. Interestingly,

the values of the quantities  $\kappa_1$ ,  $S$ ,  $S_-$ , and  $\alpha_{DFA}$  are consistent with the results deduced from a numerical simulation in fBm time series described in Ref. [18]; the latter showed that when  $\alpha_{DFA} \approx 1$  the corresponding values are  $\kappa_1 \approx 0.070$  and  $S \approx S_- \approx 0.080$ . Figure 3 depicts (with the red crosses) the most probable value  $\kappa_{1,p}$  of  $\kappa_1$  versus  $\alpha_{DFA}$  resulting from such a numerical simulation.

### III. CASE OF POWER-LAW DISTRIBUTIONS

We now study a case of self-similarity resulting from the process’ increments “infinite” variance. Here, we restrict ourselves to slowly driven systems that emit energy bursts obeying the power-law distribution

$$P(E) \sim E^{-\gamma}, \quad (4)$$

where  $\gamma$  is constant. In a large variety of such systems, in diverse fields, an inspection of the recent experimental data reveals that the  $\gamma$  exponent lies in a narrow range: i.e.,  $1.5 \leq \gamma \leq 2.1$  (and mostly even within narrower bounds: i.e.,  $\gamma = 1.5 - 1.8$ ). To realize the diversity of the phenomena that exhibit the aforementioned property, we compile some indicative examples in Table II, which are the following.

First, crystalline materials subjected to an external stress display bursts of activity owing to the nucleation and motion of dislocations. These sudden local changes produce acoustic emission waves which reveal that a large number of dislocations move cooperatively in an intermittent fashion (e.g., see [24] and references therein). As a precise example, we include in Table II the results of acoustic emission experiments on stressed single crystals of ice under viscoelastic deformation (creep), which show that the probability distribution of energy burst intensities obey a power-law distribution with  $\gamma = 1.6$  spanning many decades (see Fig. 1 of Ref. [25]). Second, the same exponent is found (i.e.,  $\gamma = 1.60 \pm 0.02$ ) [26] in the analysis of recent intermittent plastic flow observations (i.e., measurements of discrete slip events for loadings above the elastic-plastic transition) on nickel microcrystals (see Fig. 2 of Ref. [26]). Third, we consider the case of solar flares that represent impulsive energy releases in the solar corona (e.g., see Ref. [27] and references therein; see also Ref. [28] in which it is concluded that earthquakes and solar flares exhibit the same distributions of sizes, interoccurrence times, and temporal clustering). This energy release is observed in various forms: thermal, soft and hard x-ray emissions, accelerated particles, etc. The statistical analysis of these impulsive events shows that the energy distribution exhibits, over several orders of magnitude, a power law with exponents  $\gamma$  ranging from 1.5 to approximately 2.1 (depending on the experimental procedure and the geometrical assumptions adopted in the analysis). Other examples are acoustic emission from microfractures before the breakup of heterogeneous materials (wood, fiberglass), icequakes, and earthquakes.

Concerning the latter, the best known scaling relation is the Gutenberg-Richter law [29], which states that the (cumulative) number of earthquakes with magnitude greater than  $m$  occurring in a specified area and time is given by

TABLE I. The values of  $\kappa_1$ ,  $\kappa_{1,shuf}$ ,  $S$ ,  $S_-$ , and  $S_{shuf}$  for the SES activities mentioned in Ref. [15] as well as the ones (PAT and PAT<sub>2</sub>) depicted in Figs. 1 and 2, respectively. The numbers in parentheses denote the standard deviation for the distributions of  $\kappa_{1,shuf}$  and  $S_{shuf}$  in the shuffled data.

Signal	$\kappa_1$	$\kappa_{1,shuf}$	$S$	$S_-$	$S_{shuf}^b$
K1	0.063±0.003 <sup>a</sup>	0.083(0.005)	0.067±0.003 <sup>a</sup>	0.074±0.003 <sup>a</sup>	0.096(0.007)
K2	0.078±0.004 <sup>a</sup>	0.082(0.007)	0.081±0.003 <sup>a</sup>	0.103±0.003 <sup>a</sup>	0.094(0.009)
A	0.068±0.004 <sup>a</sup>	0.082(0.007)	0.070±0.008 <sup>a</sup>	0.084±0.008 <sup>a</sup>	0.092(0.010)
U	0.071±0.004 <sup>a</sup>	0.082(0.009)	0.092±0.004 <sup>a</sup>	0.071±0.004 <sup>a</sup>	0.093(0.012)
T1	0.084±0.007 <sup>a</sup>	0.082(0.007)	0.088±0.007 <sup>a</sup>	0.098±0.010 <sup>a</sup>	0.091(0.010)
C1	0.074±0.002 <sup>a</sup>	0.082(0.008)	0.083±0.004 <sup>a</sup>	0.080±0.004 <sup>a</sup>	0.092(0.011)
P1	0.075±0.004 <sup>a</sup>	0.082(0.008)	0.087±0.004 <sup>a</sup>	0.081±0.004 <sup>a</sup>	0.090(0.011)
P2	0.071±0.005 <sup>a</sup>	0.082(0.009)	0.088±0.003 <sup>a</sup>	0.072±0.015 <sup>a</sup>	0.091(0.012)
E1	0.077±0.017 <sup>a</sup>	0.083(0.008)	0.087±0.007 <sup>a</sup>	0.081±0.007 <sup>a</sup>	0.092(0.010)
PAT	0.072±0.002	0.082(0.008)	0.080±0.002	0.078±0.002	0.091(0.011)
PAT <sub>2</sub>	0.075±0.002	0.082(0.007)	0.074±0.002	0.078±0.002	0.084(0.008) <sup>c</sup>

<sup>a</sup>From Ref. [15].

<sup>b</sup>Note that  $S_{shuf}=S_{-,shuf}$  as mentioned in the text.

<sup>c</sup>This value differs from  $S_u$  because  $N=11$ ; in such a case, Eq. (A11) of Ref. [13] should be used for comparison with the “uniform” distribution.

$$N (> m) \sim 10^{-bm}, \quad (5)$$

where  $b$  is a constant, which varies only slightly from region to region [Eq. (5) holds both *regionally* and *globally*], being generally in the range  $0.8 \leq b \leq 1.2$  (see [30] and references therein). Considering that the seismic energy  $E$  released during an earthquake is related [31] to the magnitude through  $E \sim 10^{cm}$ —where  $c$  is around 1.5—Eq. (5) turns to Eq. (4), where  $\gamma=1+b/1.5$ . Hence,  $b \approx 1$  means that the exponent  $\gamma$  is around  $\gamma=1.6-1.7$ .

The following procedure is now applied: We generate (see also Ref. [32]) a large amount of artificial data obeying Eq.

(5) for a certain  $\gamma$  value. These *randomized* (“shuffled” [13]) data are subsequently analyzed, in the natural time domain, for each  $\gamma$  value, with the following procedure [17]: First, calculation of the variance  $\kappa_1$  is made for an event taking time windows for 6–40 consecutive events (the choice of the precise value of the upper limit is not found decisive, because practically the same results are obtained even if the number of consecutive events was changed from 6–40 to 6–100, as will be further discussed below). And second, this process was performed for all events by scanning the whole data set. In Fig. 4, we plot the quantity  $P(\kappa_1)$  versus  $\kappa_1$  for

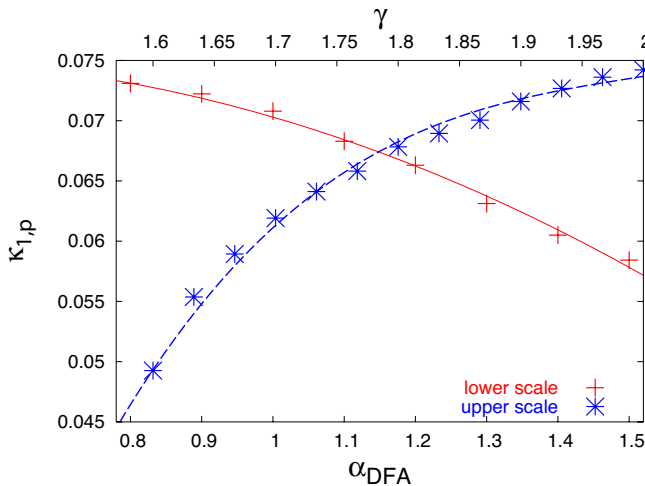


FIG. 3. (Color online) The values of  $\kappa_{1,p}$  as a function of  $\alpha_{DFA}$  for the case of the fBm simulations of Ref. [18] (red crosses, lower scale) or as a function of  $\gamma$  for power-law distributed data (blue asterisks, upper scale); see the text. They have been estimated by following the procedure described in Appendix B of Ref. [17]. The corresponding lines have been drawn as a guide to the eye.

TABLE II. Compilation of the experimental values of the power-law exponent  $\gamma$  determined in different physical processes.

Process and type of measurement	$\gamma$	References
Dislocation glide in hexagonal ice single crystals (acoustic emission)	1.6	[25]
Intermittent plastic flow in nickel microcrystals	1.6	[26]
Solar flares	1.5–2.1	[27,44–46]
Microfractures before the breakup of wood (acoustic emission)	1.51	[47,48]
Microfractures before the breakup of fiberglass (acoustic emission)	2.0	[47,48]
Earthquakes	1.5–1.8 ( $b=0.8-1.2$ )	See Ref. [30] and references therein
Icequakes	$\sim 1.8$ ( $b \approx 1.25$ )	See p. 212 of [49] and references therein

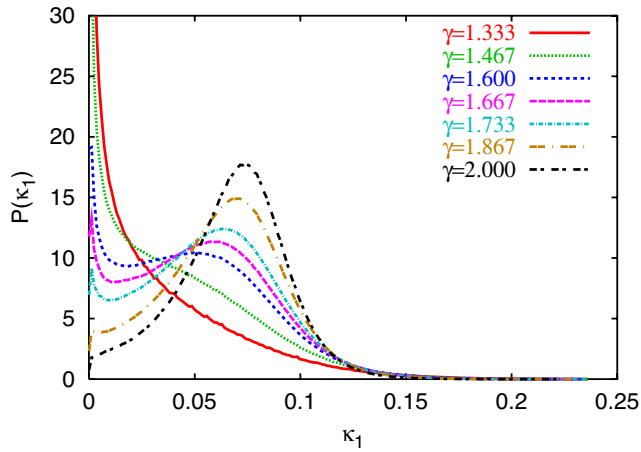


FIG. 4. (Color online) The probability density function  $P(\kappa_1)$  versus  $\kappa_1$  for several values of  $\gamma$  (see the text and Ref. [32]).

several  $\gamma$  values. The most probable value  $\kappa_{1,p}$  (for  $\gamma = \text{const}$ ) is also plotted in Fig. 3 versus the corresponding  $\gamma$  value (blue asterisks). This curve interrelates  $\kappa_1$  and  $\gamma$  for the shuffled data (thus an eventual process' memory is here destroyed [13]) and hence the plotted  $\kappa_{1,p}$  values (which differ markedly from  $\kappa_u$ ) correspond to the self-similarity resulting from the heavy-tailed distribution only.

In order to study the origin of self-similarity in a real data set, let us consider here the example of earthquakes. Using the Japan catalog mentioned in Ref. [17], we give in Fig. 5 the two curves  $P(\kappa_1)$  versus  $\kappa_1$  that result when the aforementioned calculation is made by means of a window of 6–40 consecutive events sliding through either the original catalog or a shuffled one. Comparing the resulting  $\kappa_{1,p}$  values (both of which markedly differ from  $\kappa_u$ ), we see that the value of the surrogate data ( $\approx 0.064$ ) does not greatly differ from the one ( $\approx 0.066$ ) corresponding to the original data. This may reflect that the self-similarity mainly originates from the process' increments “infinite” variance (but see also the next paragraph as well as the second paragraph of Sec.

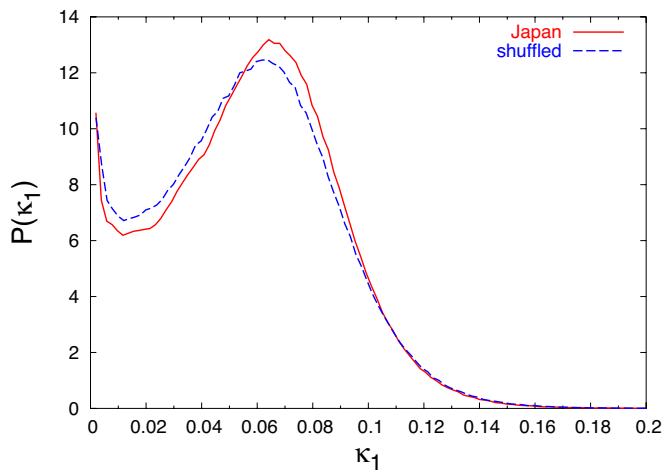


FIG. 5. (Color online) The PDF's of  $\kappa_1$  when using either the actual seismic catalog of Japan (solid red line) treated in Ref. [17] or the same data in random order (dashed blue line).

V). Note, however, that the  $\kappa_{1,p}$  value of the original data is comparable to the value  $\kappa_1 = 0.070$  that was found in infinitely ranged temporal correlations. This merits further investigation, since it may indicate the importance of temporal correlations, rather than their absence, in the earthquake catalogs.

The following clarifications are worthwhile to be mentioned. First, various aspects related to the origin of earthquake scale invariance that have been forwarded by other authors are summarized in the first sections of Refs. [17,18]. Second, when plotting  $\sigma P(X)$  vs  $(X - \langle X \rangle) / \sigma$ , where  $X$  stands for  $\Pi(\phi)$  for  $\phi \approx 0$  and  $\sigma$  its standard deviation, the following has been found [17]: for  $b$  values larger than 1 and smaller than 1.4, the curves of the surrogate data [produced on the basis of the Gutenberg-Richter law—i.e., Eq. (5)] have a general feature more or less similar to the curve of the real seismicity data. However, none of these  $b$  values in the surrogate data can lead to a curve coinciding to the one obtained from the real data. In other words, the scaled distribution reveals an *extra* complexity for the real seismic data when compared to the surrogate data, even if the latter are produced with  $b$  values comparable to the experimental ones. Third, let us now show that the method suggested in this paper does reveal (increased) temporal correlations in the well-known case of earthquake aftershocks. In this case the (modified form of) Omori law holds (e.g., Ref. [33]; see also Ref. [34] and references therein), which states that the number of aftershocks,  $dN(t)$ , occurring in the short time interval between  $t$  and  $t+dt$ , where  $t$  stands for (conventional) time elapsed after the main shock, obeys the relation

$$\frac{dN(t)}{dt} = \frac{B}{(1+t/\tau)^c}, \quad (6)$$

where  $\tau$  and  $B$  are positive constants and the exponent  $c$  is usually in the range 0.8–1.5. Using the Southern California earthquake catalog (with magnitude threshold 2.0 [17]), we now consider the aftershock series related to the Landers earthquake with magnitude 7.3 (which occurred at 11:57 UT on 28 June 1992 with an epicenter at 34.2°N 116.4°W) and the Hector Mine earthquake with magnitude 7.1 (which occurred at 09:46 UT on 16 October 1999 with an epicenter at 34.6°N 116.3°W). For these two mainshocks, Abe and Suzuki [34] identified the corresponding Omori regimes by examining the best fits of the (modified form of the) Omori law in Eq. (6) to the data based on the least-squares method. Here, we use the same aftershock data set and plot in Fig. 6 the quantity  $P(\kappa_1)$  vs  $\kappa_1$  by means of a sliding window of 6–40 consecutive events, as above, for Landers (green  $\times$ ) and Hector Mine (blue  $*$ ) earthquakes, respectively. Beyond these two aftershock series, we plot in Fig. 6 the corresponding curve (red  $+$ ) for all earthquakes that occurred within the area  $N_{32}^{37}W_{114}^{122}$  during the period 1973–2003 (this will be hereafter called SCEC [17]). Interestingly, these three curves more or less coincide and result in a common value of  $\kappa_{1,p} \approx 0.066$ , which agrees with that determined above from the original data of Japan (Fig. 5). Upon shuffling, all these three curves change, but we note that the two aftershock series (dash-dotted light blue and dotted black lines, which inter-

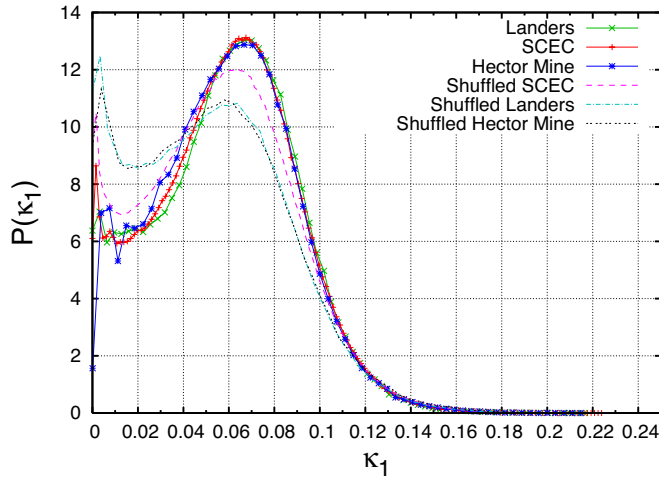


FIG. 6. (Color online) The PDF's of  $\kappa_1$  when using either the almost 30 year data of SCEC (red +) or the two aftershock series (in the Omori regime [34]) of the Landers (green  $\times$ ) and Hector Mine (blue  $*$ ) earthquakes, respectively. Note that all these three curves coincide, but they change upon shuffling (turning to dashed magenta line, dash-dotted light blue line, and dotted black line, respectively) in a way discussed in the text.

estingly also almost coincide for the surrogate data) exhibit the most noticeable change resulting in  $\kappa_{1,p} \approx 0.060$ ; on the other hand, the shuffled SCEC data (dashed magenta line) lead to  $\kappa_{1,p} \approx 0.064$  which agrees with the corresponding  $\kappa_{1,p}$  determined above from the shuffled data of Japan. In other words, when focusing on the aftershock series, we do observe that  $\kappa_{1,p}$  changes markedly upon shuffling, thus pointing to the existence of considerable temporal correlations, as it should. It seems reasonable that an Omori sequence where the events are clearly related should give better temporal correlations, and larger  $\kappa_{1,p}$  measure changes, than events in a larger earthquake catalog where there is a possibility of including unrelated events.

#### IV. MULTIPLICATIVE CASCADES: NATURAL TIME DOMAIN ANALYSIS

Here, we will study multiplicative cascades (or generalized Cantor sets [35,36]) in the natural time domain. In generalized Cantor set (multiplicative cascade), at the initial stage ( $M=1$ ) the original region is divided into  $K$  segments with possibly variable sizes, but the mass probability from the left to the right is distributed by the constant weights  $w_i$ ,  $i=1, 2, \dots, K$ , with  $\sum_i w_i = 1$ . The same procedure can then be followed in each segment at the stage  $M=2$ , etc. This is what will be hereafter called the deterministic Cantor set (DCS) in contrast to a procedure in which  $w_i$  are assigned randomly (i.e., not from the left to the right) at each segment and stage  $M$ . The latter will be called the stochastic Cantor set (SCS) and will be also studied by means of Monte Carlo simulations. A case of special practical interest is the so called  $p$  model [35] in which each segment is divided equally into two parts ( $K=2$ ), with  $w_1=p$  and  $w_2=1-p$ . This model, in its SCS flavor, was originally proposed to describe turbulence

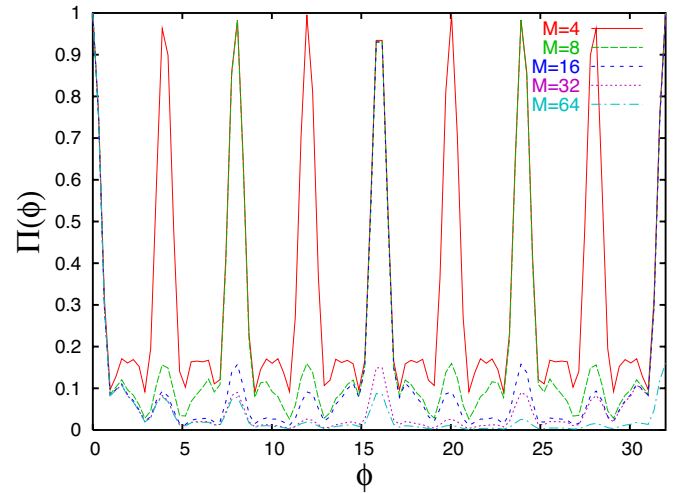


FIG. 7. (Color online)  $\Pi_M(\phi)$  for the DCS with  $K=2$  and  $p=0.3$  for  $M=4, 8, 16, 32$ , etc.

data [35,37]. Moreover, the DCS case was discussed [38] in relation to power-law time sequences in rice piles. What is important about the DCS is the following: If we consider the original region in the natural time interval  $A=[0, 1]$  ( $\chi \in A$ ) and use the obtained mass probabilities as  $p_k$  in the sense of Eq. (2), then  $\Phi(\omega) = \sum_{k=1}^N p_k \exp(i\omega \frac{k}{N})$  can be factorized and one can obtain easily the properties of the DCS in natural time. Under these conditions, for  $K=2$  and equal segments, the following relates  $\Phi_{M+1}(\omega)$  at stage  $M+1$  to that  $\Phi_M(\omega)$  at stage  $M$ :

$$\Phi_{M+1}(\omega) = \left[ p + (1-p) \exp\left(i\frac{\omega}{2}\right) \right] \Phi_M\left(\frac{\omega}{2}\right). \quad (7)$$

Equation (7) can be also generalized for  $K > 2$  into

$$\Phi_{M+1}(\omega) = \Phi_M\left(\frac{\omega}{K}\right) \sum_{j=1}^K w_j \exp\left(i\frac{(j-1)\omega}{K}\right). \quad (8)$$

Equation (7) can be also used for the calculation of  $\kappa_1$  as  $\omega$  tends to zero. A remarkable property of  $\Pi_M(\omega) = |\Phi_M(\omega)|^2$  is that, almost independently of  $M$ , all  $\Pi_M(\omega)$  have almost the same shape for natural frequencies  $\phi$  less than 0.5 (see Fig. 7). In other words, in the sense discussed above, all these stages share the same characteristic properties but differ in the high-natural-frequency range. Moreover, the application of Eq. (7) for  $\Pi_M(\omega)$  as  $\omega$  tends to zero leads to the following relation for the  $\kappa_1$  value at stage  $M+1$ :

$$\kappa_{1,M+1} = \frac{\kappa_{1,M} + p(1-p)}{4}, \quad (9)$$

which leads to

$$\kappa_{1,\infty} = \frac{p(1-p)}{3}. \quad (10)$$

Thus, for  $p=0.3$  we obtain  $\kappa_{1,\infty}=0.07$ . In Fig. 8, we compare such a DCS with the power spectrum given by Eq. (3); the results are almost identical in the region  $[0, 0.5]$ . Note, however, that the DCS does *not* satisfy the entropy  $S$  conditions

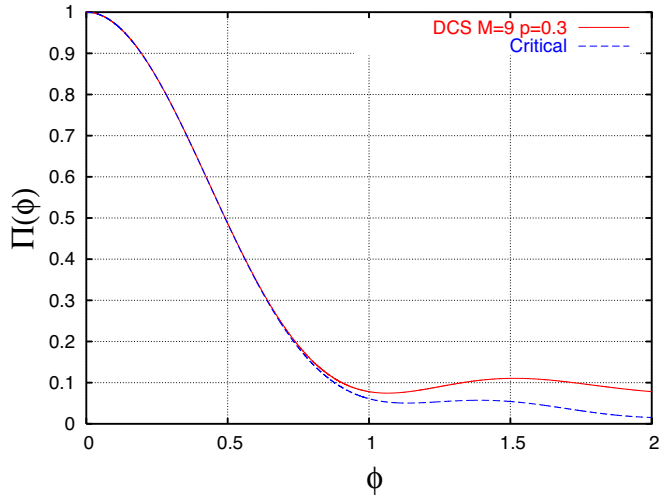


FIG. 8. (Color online) Comparison of the power spectrum of Eq. (3) (dashed blue line), with that obtained for an  $M=9$   $p$ -model DCS (solid red). The two curves are almost identical in the region  $[0,0.5]$ .

in order to be characterized as critical (see Sec. II). On the other hand, the SCS flavor of the same model, which has been proposed to describe turbulence [35,37], also gives an average  $\kappa_1 \approx 0.07$  and furthermore the entropies  $S$  and  $S_-$  for the majority of the cases treated by Monte Carlo simulations (see below) satisfy the  $S$  conditions for criticality; i.e., both  $S$  and  $S_-$  are smaller than  $S_u$  (see also Ref. [18]).

In the case of the DCS  $p$  model, the multifractal spectrum, expressed via the generalized Hurst exponent  $h(q)$ , can be found [36] to be

$$h(q) = \frac{1 - \log_2[p^q + (1-p)^q]}{q}. \quad (11)$$

Thus, one can have a relation between  $\kappa_1$  and the multifractal spectrum as was initially suggested in Ref. [12]. Figure 9 depicts the relation between  $\kappa_1$  and  $h(2)$ . As far as the stochastic case is concerned, Fig. 10 summarizes the Monte

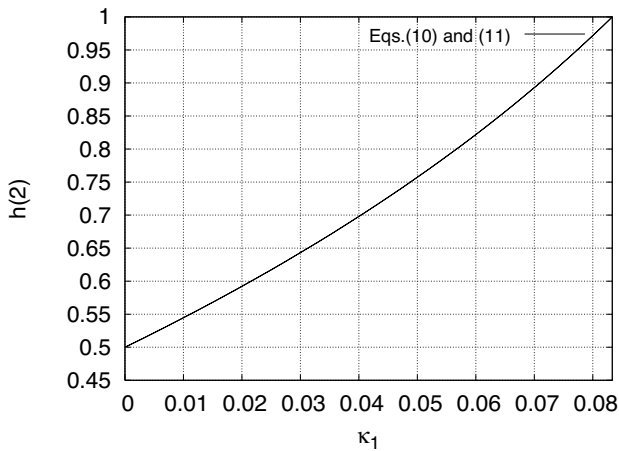


FIG. 9. The relation between  $\kappa_1$  and the generalized Hurst exponent  $h(2)$  for the DCS  $p$  model.

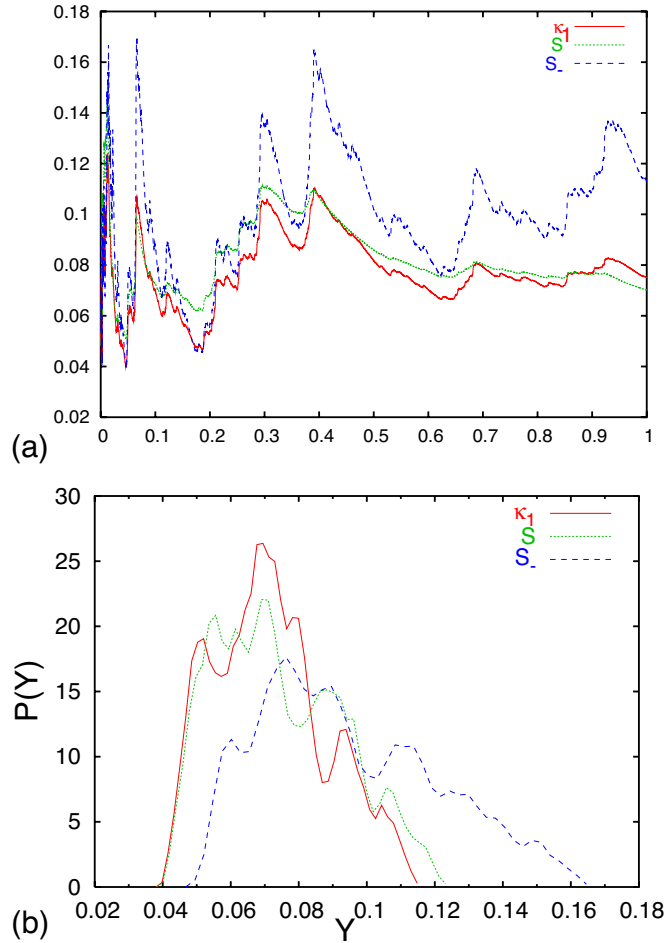


FIG. 10. (Color online) (a) A typical evolution for the SCS  $p$  model,  $p=0.3$ ; the quantities  $\kappa_1$  (solid red line),  $S$  (dotted green line), and  $S_-$  (dashed blue line) are plotted versus natural time. (b) The PDF's  $P(Y)$  of  $(Y=)\kappa_1, S, S_-$  for the case  $p=0.3$  that has been proposed to describe turbulence in Ref. [35].

Carlo study of the same model but in its SCS flavor. Interestingly, the  $\kappa_{1,p}$  value in Fig. 10 is around 0.070.

V. DISCUSSION

We first discuss the case when the increments of the series of  $Q_k$  are positive, independent, and identically distributed (PIID) variables  $r_n$  of finite variance. In this case  $Q_k = \sum_{n=1}^k r_n$  and  $Q_k$  is clearly linearly related to  $k$  on average. Thus, it is expected that the continuous distribution  $p(\chi)$ , which corresponds to  $p_k$ , is  $p(\chi) = 2\chi$ . A direct calculation then leads to the values  $\kappa_1 = \frac{1}{18} \approx 0.056 \neq \kappa_u$ ,  $S = \frac{2}{3} \ln \frac{2}{3} - \frac{2}{9} \approx 0.048 \neq S_u$ , and  $S_- = \frac{1}{3} \ln 3 - \frac{5}{18} \approx 0.088 \neq S_u$ , which significantly differ from those of the “uniform” distribution. On the other hand, when  $Q_k$  are shuffled randomly, in view of the fact that the increments have a finite variance, the distribution of  $Q_k$  for a given  $N$  has also finite variance. Thus, the results correspond to those obtained in Ref. [13] for  $Q_k$  drawn from a PIID, which lead [13] to  $S_{shuf} \rightarrow S_u$  as  $N \rightarrow \infty$ . In Appendix B, we show that also  $\kappa_{1,shuf} \rightarrow \kappa_u$  as  $N \rightarrow \infty$  (see

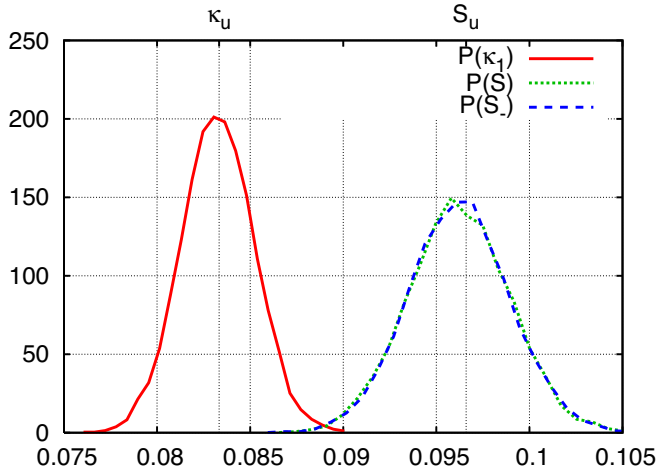


FIG. 11. (Color online) The PDF's of  $\kappa_1$ ,  $S$ , and  $S_-$ , which have been obtained by shuffling the  $Q_k$  randomly in the case of exponential increments; i.e.,  $r_n$  are randomly drawn from an exponential distribution. Here,  $N=500$  and the original time series results in  $\kappa_1=0.055$ ,  $S=0.048$ , and  $S_-=0.088$  (see the text).

also below). A numerical example for exponentially distributed increments is shown in Fig. 11.

Let us now comment on the expectation value  $E(\kappa_1)$  of  $\kappa_1$  when a (natural) time window of length  $l$  is sliding through a time series of  $Q_k \geq 0$ ,  $k=1, 2, \dots, N$ . For such a window, starting at  $k=k_0$ , the quantities  $p_j = Q_{k_0+j-1} / \sum_{m=1}^l Q_{k_0+m-1}$  are defined, and then the following relation can be proven (see Appendix B):

$$E(\kappa_1) = \kappa_{1,M} + \sum_{\text{all pairs}} \frac{(j-m)^2}{l^2} \text{Cov}(p_j, p_m), \quad (12)$$

where  $\kappa_{1,M}$  is the value of  $\kappa_1$  corresponding to the time series of the averages  $M: \{\mu_j \equiv E(p_j)\}$  and  $\text{Cov}(p_j, p_m)$  stands for the covariance of  $p_j$  and  $p_m$  defined as  $\text{Cov}(p_j, p_m) \equiv E[(p_j - \mu_j)(p_m - \mu_m)]$ , while the variance of  $p_j$  is given by  $\text{Var}(p_j) = E[(p_j - \mu_j)^2]$ . Let us first discuss the case when  $Q_k$  are shuffled randomly. Equation (12) then turns into (see Appendix B)

$$E(\kappa_{1,shuf}) = \kappa_u \left( 1 - \frac{1}{l^2} \right) - \kappa_u(l+1) \text{Var}(p) \quad (13)$$

[note that  $\text{Var}(p_j)$  is independent of  $j$ , and hence we merely write  $\text{Var}(p) \equiv \text{Var}(p_j)$ ]. If  $Q_k$  do not exhibit heavy tails and have finite variance, Eq. (13) reveals (see Appendix B) that  $E(\kappa_{1,shuf})$  rapidly converges to  $\kappa_u$ . For example, this was found in the case of the SES activities discussed in Sec. II. Otherwise,  $E(\kappa_{1,shuf})$  differs from  $\kappa_u$ , thus pointing to  $\kappa_{1,p} \neq \kappa_u$ . This is the case, for example, of the earthquakes discussed in Sec. III. Second, if  $Q_k$  do exhibit time correlations, the difference between the  $\kappa_{1,p}$  for the original and the shuffled time series most likely originates from the difference of Eqs. (12) and (13), respectively [for all the cases treated in Sec. III, this difference mainly comes from the last terms of Eqs. (12) and (13) since we verified that  $\kappa_{1,M} \approx \kappa_u$ ]. The extent to which the latter difference differs from zero

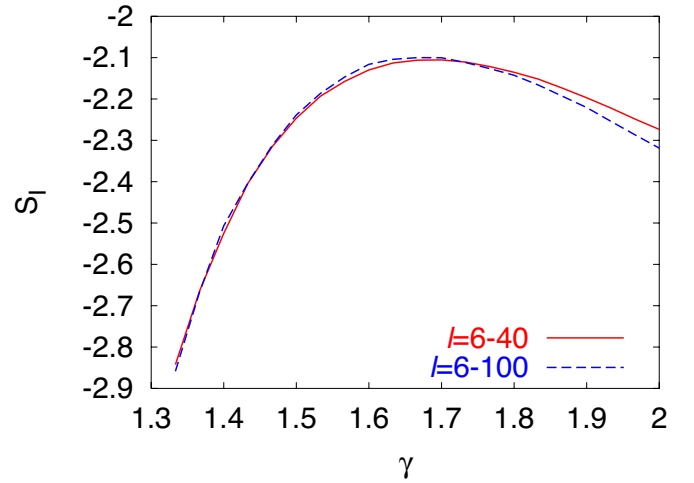


FIG. 12. (Color online) The calculated values of the differential entropy  $S_l$  versus the exponent  $\gamma$ . Two window-length ranges are used, and their results differ slightly.

accounts for the time correlations irrespective if  $Q_k$  exhibit heavy tails. For example, this is clearly the case of aftershocks and possibly the case of earthquake catalogs, in general (both of which exhibit heavy tails), discussed in Sec. III (see Figs. 5 and 6).

We now turn to a challenging point that emerges from a further elaboration of the results depicted in Fig. 4. First, note that upon increasing the  $\gamma$  value from  $\gamma=1.3$  to  $2.0$ , the feature of the curve changes significantly, becoming *bimodal* at intermediate  $\gamma$  values. Second, we calculate, for each  $\gamma$  value studied, the so-called *differential entropy*, defined as  $S_l = -\int P(\kappa_1) \ln P(\kappa_1) d\kappa_1$  which is the Shannon information entropy of a continuous probability distribution—e.g., see [39]. (Note that the Shannon information entropy is *static* entropy and *not* a dynamic one [13].) Finally, we investigate the resulting  $S_l$  values versus  $\gamma$ . Such a plot is given in Fig. 12, whose inspection reveals that  $S_l$  maximizes at a value of  $\gamma$  lying between  $\gamma=1.6$  and  $\gamma=1.7$ , which is more or less comparable with the experimental values; see Table II. (In particular for the case of earthquakes, this  $\gamma$  value corresponds to  $b \approx 1$ .) This value is not practically affected by the window length ( $l$ ) chosen, since it decreases only slightly from  $\gamma \approx 1.70$  to  $\gamma \approx 1.65$  upon increasing  $l$  from  $l=10$  to  $l=1000$ . In view of the widespread belief (e.g., [40]) that there is a close analogy between nonequilibrium phase transitions (which is likely to be [17,18] the case of earthquakes) and equilibrium ones (e.g., ferromagnetic materials)—which, however, are apparently very different problems—our study here was extended to the well-known equilibrium critical systems by investigating the Shannon entropy  $S_S \equiv -\sum_m P(m) \ln[P(m)]$ , where  $m$  denotes the order parameter, versus the temperature. Studying  $S_S$  at various temperatures, we find that it maximizes near  $T_c$  (for finite sizes  $S_S$  diverges proportionally to  $\ln N$  as  $T \rightarrow T_c$ ). For example, in Fig. 13(a) we plot the results for the following models: the infinite-range model (see Appendix C) of a ferromagnetic system of  $N$  spins ( $s_i = \pm 1$ ) (green dotted curves) and the 2D Ising (red solid curves) or 3D Ising (blue dashed curves) model. We now proceed to Fig. 13(b), which depicts, as an example,

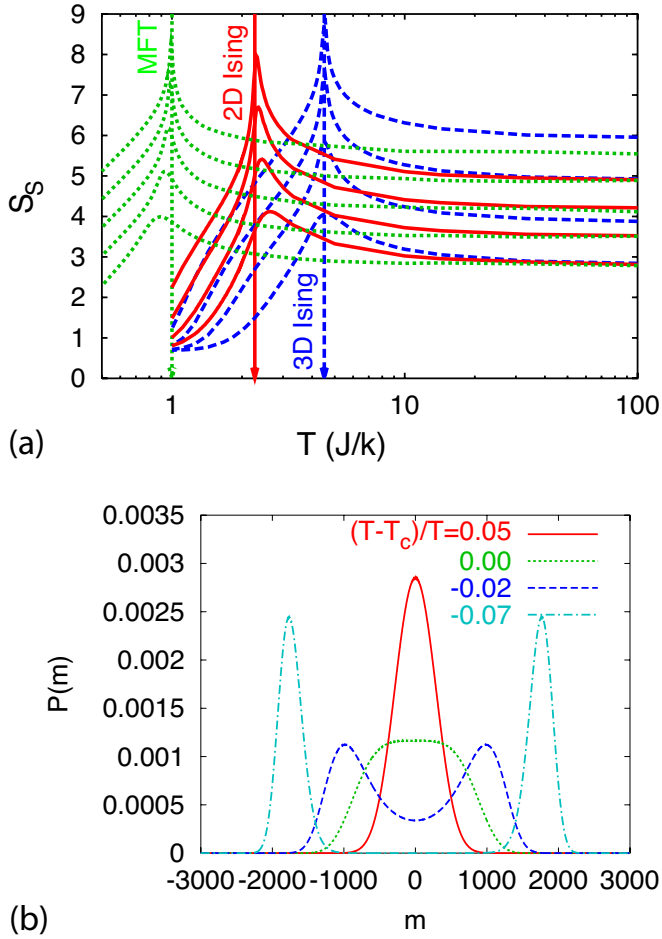


FIG. 13. (Color online) (a) The Shannon entropy  $S_S \equiv -\sum_m P(m) \ln[P(m)]$  versus  $T$  calculated for the following equilibrium critical models: infinite-range model Hamiltonian for a ferromagnetic system of  $N=2^n$  spins (MFT, dotted green line,  $n=6, 8, 10, 12$ , and 14), two-dimensional line Ising (solid red line,  $n=6, 8, 10$ , and 12) and three-dimensional Ising (dashed blue line,  $n=6, 9, 12$ , and 15); in each case, the results are given for various sizes, increasing from bottom to top ( $S_S$  diverges as  $\ln N$ ). (b) The probability density  $P(m)$  versus the order parameter  $m$  for four values of the quantity  $(T-T_c)/T$  for the infinite-range model with  $N=4096$ .

$P(m)$  for the first model at various temperatures above and below the critical temperature  $T_c$ , for  $N=4096$  spins. Note that *just* below  $T_c$  a bimodal feature emerges, which is reminiscent of the one found in Fig. 4 (for intermediate  $\gamma$  values). This inspired us to discuss the slight variation of the  $\gamma$  value (at which  $S_I$  maximizes in Fig. 12) versus  $l$  by means of a procedure analogous to well-known finite-size scaling techniques. Indeed, in Fig. 14(a) we plot for three different  $l$  the  $P(\kappa_1)$  that arises when  $S_I$  is approaching its maximum. These three PDF's almost coincide, pointing to a common bimodal PDF. The latter, of course, is described by a single average value  $E(\kappa_1)$ , labeled  $\mu$ , and variability  $\sigma/\mu$  (where  $\sigma$  stands for the standard deviation of  $\kappa_1$ ). The latter two values are depicted with the horizontal solid lines in Figs. 14(b) and 14(c), respectively. The appearance of the common bimodal PDF of Fig. 14(a), and hence the maximization of  $S_I$ , can be

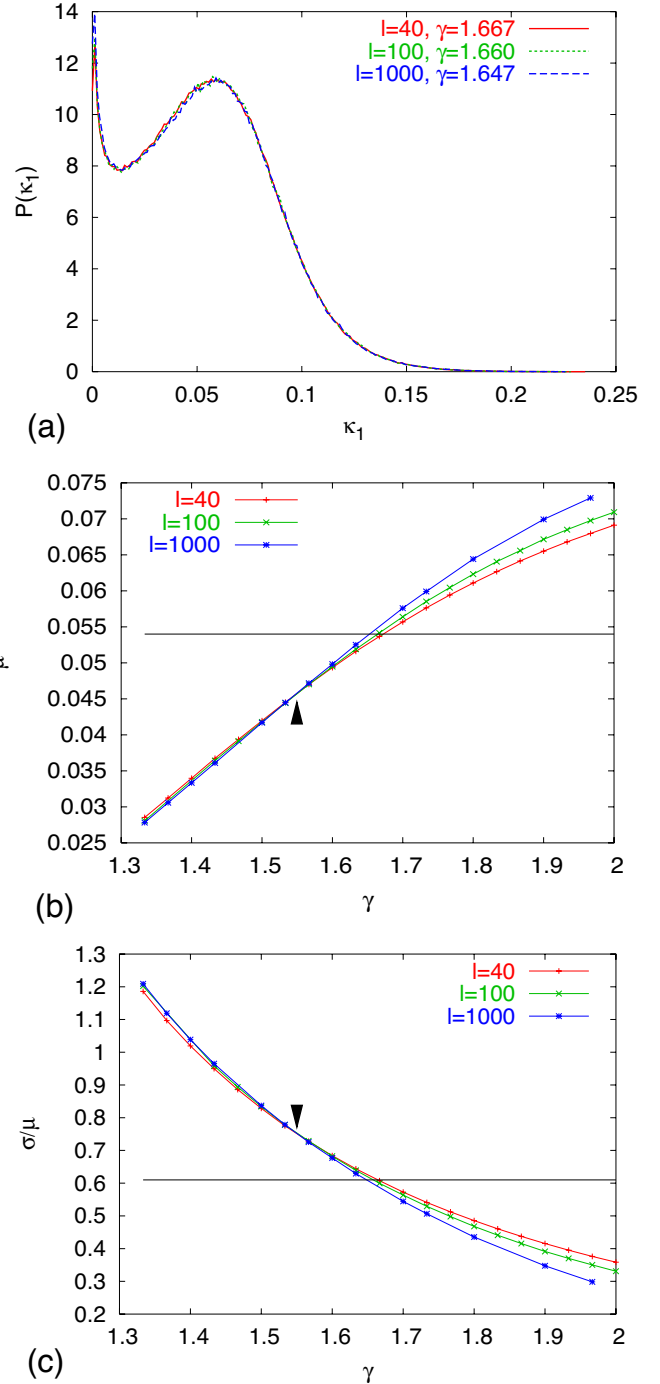


FIG. 14. (Color online) (a) The bimodal feature of  $P(\kappa_1)$  when  $S_I$  is approaching its maximum value. Three different values of  $l$  are shown. (b), (c) depict the average value  $E(\kappa_1)$ , labeled  $\mu$  and the variability  $\sigma/\mu$  (where  $\sigma$  stands for the standard deviation of  $\kappa_1$ ) versus  $\gamma$ , respectively. The horizontal solid lines correspond to the average value and the variability of the bimodal PDF shown in (a). We observe that in (b) and (c) the curves for various  $l$  intersect at  $\gamma_c \approx 1.55$ , shown by the arrows (see the text).

deduced by comparing the mean value and variability of  $\kappa_1$  for several  $l$  values as  $\gamma$  varies. This comparison is made in Figs. 14(b) and 14(c), the study of which shows that the curves for different  $l$  intersect at  $\gamma_c \approx 1.55$ . Note that as  $l$

increases the curves become steeper; thus,  $\gamma_c$  provides a lower bound for the  $\gamma$  value that maximizes  $S_l$  as  $l \rightarrow \infty$ .

Does the above finding in Fig. 12 mean that the  $b$  or  $\gamma$  value can be determined just by applying the maximum entropy principle in the sense developed by Jaynes [41,42], who suggested to look at statistical mechanics as a form of *statistical inference* and *start* statistical physics from the principle of maximum entropy inference (MaxEnt)? This is not yet clear, because a widely accepted formalism for *non-equilibrium* statistical mechanics is still lacking. The fact that in some experiments the resulting  $\gamma$  values differ slightly from  $\gamma=1.6$  to  $1.7$  predicted from Fig. 12 could be attributed to the following: Figure 12 is based on randomized data, while the actual data may also exhibit temporal correlations (e.g., the case of aftershocks). In addition, finite-size effects [8] might play a significant role.

## VI. MAIN CONCLUSIONS

In summary, the origin of self-similarity may be distinguished as follows: If self-similarity exclusively results from the process' memory, the  $\kappa_1$  value should *change* to  $\kappa_u=0.0833$  (and the values of  $S$ ,  $S_-$  to  $S_u=0.0966$ ) for the (randomly) shuffled data. This is the case of the SES activities. On the other hand, if the self-similarity results from process' increments "infinite" variance *only*, the  $\kappa_{1,p}$  values should be the same (but differing from  $\kappa_u$ ) for the original and (randomly) shuffled data. The example of earthquakes investigated does not fully conform to the latter case most likely due to the presence of temporal correlation.

When studying the differential entropy associated with the PDF of  $\kappa_1$ , it maximizes when the exponent  $\gamma$  in Eq. (4) lies in the narrow range  $\approx 1.6-1.7$ , in agreement with the experimental findings in diverse fields. This, for the case of earthquakes, immediately reflects the fact that the  $b$  value in the Gutenberg-Richter law is  $b \approx 1$ , as actually observed.

## APPENDIX A: DETERMINATION OF THE OCCURRENCE TIME OF AN IMPENDING SEISMIC ACTIVITY

In the initial submission of the present paper on 25 February 2006, the signal in Fig. 1(a) had been classified as SES activity. Actually, on 3 April 2006 a strong seismic activity started with an earthquake of magnitude 5.3 in a region 80–100 km west of PAT station, at which the SES activity had been recorded. The occurrence time of the initiation of this earthquake activity (which lasted until 19 April 2006 with earthquakes of magnitude up to 5.9) can be specified within a narrow range around 2 days, by computing the order parameter of seismicity [17] (see Sec. I), as explained in detail in Ref. [20].

## APPENDIX B: THE EXPECTATION VALUE OF $\kappa_1$ FOR A GIVEN WINDOW LENGTH $l$

Here, we focus on the expectation value  $E(\kappa_1)$  when sliding a (time) window of length  $l$  through a time series of  $Q_k \geq 0$ ,  $k=1, 2, \dots, N$ . In a window of length  $l$  starting at  $k$

$=k_0$ , the quantities  $p_j = Q_{k_0+j-1} / \sum_{m=1}^l Q_{k_0+m-1}$  are obtained, which satisfy the necessary conditions

$$p_j \geq 0, \quad (\text{B1})$$

$$\sum_{j=1}^l p_j = 1, \quad (\text{B2})$$

to be considered as point probabilities. We then define [9,11] the moments of the natural time,  $\chi_j = j/l$  as  $\langle \chi^q \rangle = \sum_{j=1}^l (j/l)^q p_j$ , and hence

$$\kappa_1 = \sum_{j=1}^l \left( \frac{j}{l} \right)^2 p_j - \left[ \sum_{j=1}^l \frac{j}{l} p_j \right]^2. \quad (\text{B3})$$

Note that  $\kappa_1$  is a nonlinear functional of  $\{p_j\}$ . Let us consider the expectation value  $\mu_j \equiv E(p_j)$  of  $p_j$ . For the purpose of our calculation the relation between the variance of  $p_j$ ,  $\text{Var}(p_j) \equiv E((p_j - \mu_j)^2)$ , and the covariance of  $p_j$  and  $p_m$ ,  $\text{Cov}(p_j, p_m) \equiv E((p_j - \mu_j)(p_m - \mu_m))$  is important. In view of Eqs. (B1) and (B2), the quantities  $\mu_j$ ,  $\text{Var}(p_j)$ , and  $\text{Cov}(p_j, p_m)$  are always finite, independent of the presence of heavy tails in  $Q_k$ . Using the constraint (B2), leading to  $p_j - \mu_j = \sum_{m \neq j} (\mu_m - p_m)$ , we obtain

$$\text{Var}(p_j) = - \sum_{m \neq j} \text{Cov}(p_j, p_m). \quad (\text{B4})$$

We now turn to the evaluation of  $E(\kappa_1)$  and study its difference from the one that corresponds to the average time series  $\mathbb{M} = \{\mu_k\}$  which is labeled  $\kappa_{1,\mathbb{M}}$ . Hence,

$$\begin{aligned} E(\kappa_1) - \kappa_{1,\mathbb{M}} &= E \left[ \sum_{m=1}^l \frac{m^2}{l^2} (p_m - \mu_m) - \left( \sum_{m=1}^l \frac{m}{l} p_m \right)^2 + \left( \sum_{m=1}^l \frac{m}{l} \mu_m \right)^2 \right]. \end{aligned} \quad (\text{B5})$$

In view of the definition of  $\mu_m$ , the first term on the right-hand side of Eq. (B5) vanishes, whereas the latter two terms reduce to the variance of  $\langle \chi \rangle$ :

$$E(\kappa_1) - \kappa_{1,\mathbb{M}} = - E \left( \left[ \sum_{m=1}^l \frac{m}{l} (p_m - \mu_m) \right]^2 \right). \quad (\text{B6})$$

Expanding this variance, we get

$$\kappa_{1,\mathbb{M}} - E(\kappa_1) = \sum_{m=1}^l \frac{m^2}{l^2} \text{Var}(p_m) + 2 \sum_{j=1}^{l-1} \sum_{m=j+1}^l \frac{jm}{l^2} \text{Cov}(p_j, p_m), \quad (\text{B7})$$

which, upon using Eq. (B4), leads to

$$\begin{aligned} E(\kappa_1) - \kappa_{1,\mathbb{M}} &= \sum_{j=1}^{l-1} \sum_{m=j+1}^l \frac{(j-m)^2}{l^2} \text{Cov}(p_j, p_m) \\ &= \frac{1}{2} \sum_{j=1}^l \sum_{m=1}^l \frac{(j-m)^2}{l^2} \text{Cov}(p_j, p_m). \end{aligned} \quad (\text{B8})$$

This relation turns into

$$E(\kappa_1) = \kappa_{1,M} + \sum_{\text{all pairs}} \frac{(j-m)^2}{l^2} \text{Cov}(p_j, p_m), \quad (\text{B9})$$

where  $\sum_{\text{all pairs}} \equiv \sum_{j=1}^{l-1} \sum_{m=j+1}^l$ . Equation (B9) is just Eq. (12) of the main text.

From there on we assume that  $Q_k$  do not exhibit time correlations, which is the case, for example, of randomly shuffled data. As the window is sliding throughout the whole time series,  $Q_k$  take, of course, every position  $j$  within the window of length  $l$ . Then, Eq. (B2) leads to

$$E(p_j) = \frac{1}{l}, \quad (\text{B10})$$

and  $\text{Cov}(p_j, p_m)$  becomes independent of  $j$  and  $m$ , and Eq. (B4) then leads to  $\text{Cov}(p_j, p_m) = -\text{Var}(p)/(l-1)$  [ $\text{Var}(p_j)$  is also independent of  $j$ , and for this reason  $\text{Var}(p_j)$  was merely substituted by  $\text{Var}(p)$ ]. Moreover,  $\kappa_{1,M}$  reduces to  $\kappa_{1,c}$ , where  $\kappa_{1,c}$  corresponds to the constant time series  $\mathbb{K} = \{x_k : x_k = 1/l, k=1, 2, \dots, l\}$ , which is given by

$$\kappa_{1,c} = \sum_{m=1}^l \frac{m^2}{l^3} - \left( \sum_{m=1}^l \frac{m}{l^2} \right)^2 = \kappa_u \left( 1 - \frac{1}{l^2} \right), \quad (\text{B11})$$

where  $\kappa_u = 1/12 \approx 0.0833$ . Turning now to Eq. (B7) and by adding and subtracting  $\frac{\text{Var}(p)}{l-1} \sum \frac{m^2}{l^2}$ , we obtain, for the *shuffled* data,

$$E(\kappa_1) = \kappa_u \left( 1 - \frac{1}{l^2} \right) - \kappa_u(l+1)\text{Var}(p), \quad (\text{B12})$$

which is just Eq. (13) of the main text. In view of Eqs. (B1) and (B2),  $\text{Var}(p) < E(p^2) < E(p) = 1/l$ , and thus the second

term in Eq. (B12) remains finite for  $l \rightarrow \infty$ . If  $Q_k$  do not exhibit heavy tails and have finite variance,  $\text{Var}(p)$  scales [13] as  $1/l^2$  and thus  $E(\kappa_1)$  rapidly converges to  $\kappa_u$ , validating the criterion suggested in Sec. II. Otherwise, the expectation value of  $\kappa_1$  of the shuffled data differs from  $\kappa_u$ , thus pointing to  $\kappa_{1,p} \neq \kappa_u$  and hence detects the presence of heavy tails in the examined time series.

### APPENDIX C: THE INFINITE-RANGE MODEL OF A FERROMAGNETIC SYSTEM OF $N$ SPINS ( $s_i = \pm 1$ )

The Hamiltonian for such a system is given by ( $J > 0$ )  $H = -\frac{Jm^2}{2N}$  where  $m = \sum_{i=1}^N s_i$  is the total magnetization. This system, which undergoes a second-order phase transition at  $T_c = J/k$  (where  $k$  is the Boltzmann constant), is exactly solvable by the mean-field theory (e.g., [43]). The degeneracy  $g(m)$  of a state with a given  $m$  is just the number of combinations one can flip  $(N-m)/2$  out of  $N$  spins:

$$g(m) = \frac{N!}{\left(\frac{N-m}{2}\right)! \left(\frac{N+m}{2}\right)!}, \quad (\text{C1})$$

resulting in a canonical (ensemble) point probability

$$P(m) = \frac{g(m) \exp\left(\frac{Jm^2}{2NkT}\right)}{\sum_n g(n) \exp\left(\frac{Jn^2}{2NkT}\right)}, \quad (\text{C2})$$

where the summation is over all the possible values of  $m$ . Equation (C2) was used to obtain the results plotted in Fig. 13(b).

- 
- [1] C.-K. Peng, S. Havlin, and H. E. Stanley, *Chaos* **5**, 82 (1995).  
[2] T. Kalisky, Y. Ashkenazy, and S. Havlin, *Phys. Rev. E* **72**, 011913 (2005).  
[3] J. W. Lampeti, *Trans. Am. Math. Soc.* **104**, 62 (1962).  
[4] A. Weron, K. Burnecki, S. Mercik, and K. Weron, *Phys. Rev. E* **71**, 016113 (2005).  
[5] C. Tsallis, S. V. F. Levy, A. M. C. Souza, and R. Maynard, *Phys. Rev. Lett.* **75**, 3589 (1995).  
[6] C. Tsallis, S. V. F. Levy, A. M. C. Souza, and R. Maynard, *Phys. Rev. Lett.* **77**, 5442 (1996).  
[7] N. Scaffeta and B. J. West, *Complexity* **10**(4), 51 (2005).  
[8] M. Ausloos and R. Lambiotte, *Phys. Rev. E* **73**, 011105 (2006).  
[9] P. A. Varotsos, N. V. Sarlis, and E. S. Skordas, *Practica Athens Acad.* **76**, 294 (2001).  
[10] P. A. Varotsos, N. V. Sarlis, and E. S. Skordas, *Phys. Rev. E* **66**, 011902 (2002).  
[11] P. A. Varotsos, N. V. Sarlis, and E. S. Skordas, *Phys. Rev. E* **67**, 021109 (2003).  
[12] P. A. Varotsos, N. V. Sarlis, and E. S. Skordas, *Phys. Rev. E* **68**, 031106 (2003).  
[13] P. A. Varotsos, N. V. Sarlis, E. S. Skordas, and M. S. Lazaridou, *Phys. Rev. E* **70**, 011106 (2004).  
[14] P. A. Varotsos, N. V. Sarlis, E. S. Skordas, and M. S. Lazaridou, *Phys. Rev. E* **71**, 011110 (2005).  
[15] P. A. Varotsos, N. V. Sarlis, H. K. Tanaka, and E. S. Skordas, *Phys. Rev. E* **71**, 032102 (2005).  
[16] P. Varotsos, *The Physics of Seismic Electric Signals* (TERRA-PUB, Tokyo, 2005).  
[17] P. A. Varotsos, N. V. Sarlis, H. K. Tanaka, and E. S. Skordas, *Phys. Rev. E* **72**, 041103 (2005).  
[18] P. A. Varotsos, N. V. Sarlis, E. S. Skordas, H. K. Tanaka, and M. S. Lazaridou, *Phys. Rev. E* **73**, 031114 (2006).  
[19] H. Tanaka, P. A. Varotsos, N. V. Sarlis, and E. S. Skordas, *Proc. Jpn. Acad., Ser. B: Phys. Biol. Sci.* **80**, 283 (2004).  
[20] See EPAPS document No. E-PLLEE8-74-190608 for additional information. For more information on EPAPS, see <http://www.aip.org/pubservs/epaps.html>.  
[21] See EPAPS Document No. E-PLLEE8-68-116309 for additional information, originally from P. A. Varotsos, N. V. Sarlis, E. S. Skordas, *Phys. Rev. E* **68**, 031106 (2003). For more information on EPAPS, see <http://www.aip.org/pubservs/epaps.html>.  
[22] C.-K. Peng, S. V. Buldyrev, S. Havlin, M. Simons, H. E. Stan-

- ley, and A. L. Goldberger, *Phys. Rev. E* **49**, 1685 (1994).
- [23] S. V. Buldyrev, A. L. Goldberger, S. Havlin, R. N. Mantegna, M. E. Matsu, C.-K. Peng, M. Simons, and H. E. Stanley, *Phys. Rev. E* **51**, 5084 (1995).
- [24] M. Koslowski, R. LeSar, and R. Thomson, *Phys. Rev. Lett.* **93**, 125502 (2004).
- [25] M.-C. Miguel, A. Vespignani, S. Zapperi, J. Weiss, and J. R. Grasoo, *Nature (London)* **410**, 667 (2001).
- [26] D. M. Dimiduk, C. Woodward, R. LeSar, and M. D. Uchic, *Science* **312**, 1188 (2006).
- [27] G. Nigro, F. Malara, V. Carbone, and P. Veltri, *Phys. Rev. Lett.* **92**, 194501 (2004).
- [28] L. de Arcangelis, C. Godano, E. Lippiello, and M. Nicodemi, *Phys. Rev. Lett.* **96**, 051102 (2006).
- [29] B. Gutenberg and C. F. Richter, *Seismicity of the Earth and Associated Phenomena* (Princeton University Press, Princeton, 1954).
- [30] J. B. Rundle, D. L. Turcotte, R. Shcherbakov, W. Klein, and C. Sammis, *Rev. Geophys.* **41**, 1019 (2003).
- [31] H. Kanamori, *Nature (London)* **271**, 411 (1978).
- [32] The curves of Fig. 4 for the case of earthquakes can be obtained as follows: We first generate, for each  $b$  value, artificial data that obey the Gutenberg-Richter relation  $N(>m) \sim 10^{-bm}$  above a certain magnitude threshold (e.g.,  $m \geq 0$ ). This was repeated for various  $b$  values by keeping the total number (500 000) of events *constant* (which implies that when changing the  $b$  value, the maximum magnitude  $m_{max}$  involved in the calculation also changes). These data were subsequently analyzed in natural time, for each  $b$  value, with the procedure described in the text as well as in P. Varotsos *et al.*, *Proc. Jpn. Acad., Ser. B: Phys. Biol. Sci.* **80**, 429 (2004).
- [33] P. A. Reasenber and L. M. Jones, *Science* **243**, 1173 (1989).
- [34] S. Abe and N. Suzuki, *Physica A* **332**, 533 (2004).
- [35] C. Meneveau and K. R. Sreenivasan, *Phys. Rev. Lett.* **59**, 1424 (1987).
- [36] H. Chen, X. Sun, H. Chen, Z. Wu, and B. Wang, *New J. Phys.* **6**, 84 (2004).
- [37] J. O'Neil and C. Meneveau, *Phys. Fluids A* **5**, 158 (1993).
- [38] R. Pastor-Satorras, *Phys. Rev. E* **56**, 5284 (1997).
- [39] R. Garbaczewski, *Entropie* **7**, 253 (2005).
- [40] M.-C. Miguel and S. Zapperi, *Science* **312**, 1151 (2006).
- [41] E. T. Jaynes, *Phys. Rev.* **106**, 620 (1957).
- [42] E. T. Jaynes, *Probability Theory: The Logic of Science* (Cambridge University Press, New York, 2003).
- [43] L. P. Kadanov, *Statistical Physics: Statics, Dynamics and Renormalization* (World Scientific, Singapore, 2000).
- [44] M. J. Aschwanden *et al.*, *Astrophys. J.* **535**, 1047 (2000).
- [45] E. N. Parnell and P. E. Jupp, *Astrophys. J.* **529**, 554 (2000).
- [46] D. Hughes, M. Paczuski, R. O. Dendy, P. Helander, and K. G. McClements, *Phys. Rev. Lett.* **90**, 131101 (2003).
- [47] A. Garcimartin, A. Guarino, L. Bellon, and S. Ciliberto, *Phys. Rev. Lett.* **79**, 3202 (1997).
- [48] A. Guarino, S. Ciliberto, A. Garcimartin, M. Zei, and R. Scorzetti, *Eur. Phys. J. B* **26**, 141 (2002).
- [49] J. Weiss, *Surv. Geophys.* **24**, 185 (2003).